Intersubband transitions of a quasi-two-dimensional electron gas in the strong disorder regime

C. Metzner, M. Hofmann, and G. H. Döhler
Institut für Technische Physik I, Universität Erlangen, Erwin-Rommel-Straße 1, 91058 Erlangen, Germany
(Received 2 February 1998; revised manuscript received 14 April 1998)

In modulation δ-doped quantum wells with thin spacer layers the electrons are localized by strong doping-induced potential fluctuations. We analyze in detail the corresponding single-particle wave functions by a direct numerical solution of the multisubband quasi-two-dimensional Schrödinger equation and calculate the intersubband absorption spectra. Although the disorder-induced broadening of the density of states is strong, we only find a small linewidth for the intersubband transitions in the case of thin quantum wells. This behavior can be traced back to a strong spatial correlation between the states associated with the ground and first excited subband of the undisturbed system. For thicker wells the subband mixing increases and a gradual, asymmetric broadening of the absorption peak is found. These results are compared to a simple, semiclassical approximation. It is demonstrated that the correlation between energetically separated quantum states is one of the key effects of the intersubband excitation process, which is also relevant for other fields dealing with strongly disordered multisubband systems. [S0163-1829(98)01436-2]

I. INTRODUCTION

The peak position and line shape of the intersubband resonance in quantum wells has been the subject of extensive studies during recent years.[1] The experimentally observed resonance energy and finite linewidth has been explained by the interplay of various effects related to the complex band structure of the host semiconductor and to the electron-electron interaction.

In an idealized system without growth imperfections or charged impurities, with a parabolic in-plane dispersion relation and neglecting many-body corrections, the absorption peak would resemble a δ function at a position equal to the subband energy difference, corresponding to k-conserving transitions of electrons from the ground subband to the first excited subband. In nonparabolic bands the electrons in different subbands have different dispersion relations and thus the transition energy becomes k dependent. This already leads to a temperature- and density-dependent broadening of the absorption peak.[5] At higher electron densities many-body effects play an important role in the absorption process.[2] The dynamic screening of the perturbing light field by the electrons (depolarization) causes a blueshift of the resonance peak, which is partly compensated for by the excitonic attraction between the excited electrons and holes left back in the ground subband.[6] In combination with the band nonparabolicity, this gives also rise to an additional line distortion.[7]

The broadening of the absorption peak by disorder effects, such as interface roughness[3] or doping-induced potential fluctuations,[4] is usually included only by comparatively coarse approximations,[8] or simply by introducing an empirical broadening parameter. This approach may be justified for high-quality modulation-doped quantum wells at high electron density, where the disorder is small from the start or due to effective screening by the electron gas. In samples with small spacer layer thickness, however, the potential fluctuations become very large when the electrons in the quantum well are depleted.[9] The remaining electrons are typically localized at the minima of the random potential and neither the wave vector nor the subband number are good quantum numbers anymore. It can be expected that in this regime the intersubband absorption spectrum is mainly determined by the disorder effect. Therefore in this paper we investigate in detail the effect of doping-induced potential fluctuations on the far-infrared absorption spectra of a modulation-doped quantum well, due to single-electron transitions within the conduction band (CB).

The organization of the paper is as follows. In Sec. II we introduce the model system with its parameters and the fundamental assumptions. The following Sec. III is devoted to describing the two different simulation approaches used for calculating the quantum states and absorption spectra. The results of the simulations are then presented and discussed in detail in Sec. IV. Finally we summarize the physical insight gained by our simulations in Sec. V.

II. MODEL SYSTEM

The main purpose of this paper is to clarify the general structure of the quantum states in a multisubband quasi-2D electron gas subject to a disorder potential of controllable magnitude. This situation can be realized experimentally in various types of devices, the most prominent being modulation-doped heterostructures.

In this case, the two-dimensional confinement of the electron gas can be provided by a simple heterojunction or by a quantum well and the doping may be extended over a finite volume or restricted to a single monolayer. The carrier density may be varied by optical excitation or by using electrical contacts, as in field-effect transistor structures.

To avoid any nonessential complication, we use an idealized model system for our calculations, in which all secondary, device-related features are ignored. We thus consider the 2D electron gas to be confined within an infinitely deep quantum well (QW) of thickness a, defining its potential as $V_{qw}(z)=0$ for $0<z<a$ and $V_{qw}(z)=\infty$ elsewhere.

Our coordinate system is such that the z-axis points along the growth direction (vertical to the layers), with $z=0$ at the

 © 1998 The American Physical Society

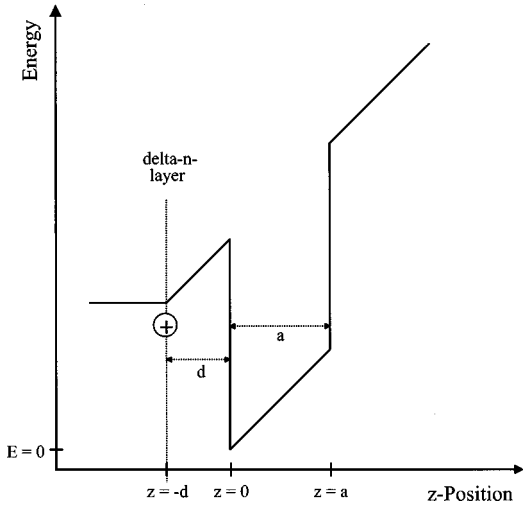

FIG. 1. Schematic band-edge diagram of our model system: a modulation δ-doped quantum well (QW). In the calculation we assumed infinitely high barriers.

left quantum well boundary. The coordinates x,y are referred to as lateral positions and summarized as $\vec{r}$.

The positively charged donor impurities with sheet density $N_D^{(2)}$ are assumed to be distributed statistically within a δ-doping monolayer, separated from the left well boundary by a spacer layer of thickness d (compare Fig. 1). They produce a random Coulomb potential $V_{imp}(z,\vec{r})$ in the QW region, the short wave components of which grow exponentially with decreasing d. The total potential profile experienced by the electrons is thus given by

$$V_{tot}(z,\vec{r}) = V_{qw}(z) + V_{imp}(z,\vec{r}). \tag{1}$$

We can only cope with a finite lateral segment of the ideally infinite system in our numerical simulation. We thus choose a quadratic simulation area of linear extension L and use two-side periodic boundary conditions to minimize finite-size effects. In principle, this changes the system into a planar superlattice with a very complicated unit cell. Consequently, the resulting eigenstates should be of Bloch type and minibands should be formed in the energy spectrum. However, the wave functions of the low-energy states considered below are all strongly localized with a localization length smaller than L. Therefore, quantum overlap between neighboring unit cells is exponentially small and the resulting miniband width can be neglected. Although we calculate only the Bloch functions at the bottom of each miniband, these represent almost perfectly the states of the infinite system. The approximation can of course be improved arbitrarily by increasing the size of the unit cell, which is only limited by computational resources. We used $L=100$ nm for our simulations and have made sure that our results are insensitive to a further increase of L. For the material parameters we used the electron mass and dielectric constant of GaAs with $m^*=0.065m_0$ and $\epsilon=12.5$.

The Coulomb potential of the n-doping layer can be decomposed into its lateral average and a fluctuating part:

$$V_{imp}(z,\vec{r}) = eF_D z + V_{fl}(z,\vec{r}) \quad \text{with} \quad \langle V_{fl}(z,\vec{r})\rangle_{\vec{r}} = 0. \tag{2}$$

The electric field F_D is assumed to be zero left from the n layer and constant $F_D = 4\pi K_0 N_D^{(2)}$ to the right, thus neglecting screening and band bending effects. Here $K_0 = e^2/(4\pi\epsilon\epsilon_0)$ is the Coulomb constant. Performing a lateral Fourier transform we can write

$$V_{imp}(z,\vec{q}) = \delta_{\vec{q},\vec{0}} eF_D z + (1-\delta_{\vec{q},\vec{0}}) V_{fl}(z,\vec{q}). \tag{3}$$

The potential fluctuations can be factorized into a single impurity term and a form factor depending on the lateral donor positions $\vec{r}_i$. For wave vectors consistent with the periodic boundary conditions, $\vec{q}=(2\pi/L)(u,v)$ with the u,v integer, we can write

$$V_{fl}(z,\vec{q}) = V_0(z,q)\cdot S(\vec{q}) = \frac{-2\pi K_0}{q} e^{-q(z+d)} (1/L^2) \sum_i e^{-i\vec{q}\vec{r}_i}. \tag{4}$$

It should be noted that it would be straightforward to extend the calculations presented in this paper to realistic device structures, including finite barrier heights and self-consistent band bending effects, thus enabling a direct comparison to experimental results. Also the (generally nonlinear) screening in a strictly two-dimensional electron gas has already been investigated in detail in Ref. 9 and the application of this theory to quasi-2D multisubband systems bears no fundamental difficulties.

III. THEORETICAL APPROACHES

A. Preliminary remarks

For the later discussion it will be useful to reflect the effects of the different potential contributions on the electrons step by step. We start with the undisturbed Hamiltonian, defined by the pure quantum well without any doping induced potentials:

$$H_0 = H_0^z + (\mathbf{p}_r^2/2m^\star) = [(p_z^2/2m^\star) + V_{qw}(z)] + (\mathbf{p}_r^2/2m^\star) \tag{5}$$

and its eigenstates

$$H_0 \varphi_\mu^0(z) e^{i\vec{k}\vec{r}} = \left(\epsilon_\mu^0 + \frac{\hbar^2 k^2}{2m^\star}\right) \varphi_\mu(z) e^{i\vec{k}\vec{r}}, \tag{6}$$

with

$$\varphi_\mu^0(z) = (\sqrt{2/a})\sin(\mu\pi z/a),$$

$$\epsilon_\mu^0 = \left(\frac{\hbar^2\pi^2}{2m^\star a^2}\right)\mu^2 \quad \text{and} \quad \mu = 1,2,\ldots. \tag{7}$$

If we now add the homogeneous electric field term to the undisturbed Hamiltonian,

$$H_1 = H_0 + eF_D z, \tag{8}$$

we have a situation well known as the longitudinal Stark effect in quantum wells, which is usually discussed in connection with the interband exciton. The $\vec{r}$-independent elec-

tric field leads merely to a shift of the subband edges and to a deformation of the z wave functions,

$$\epsilon_\mu^0 \to \epsilon_\mu^1, \quad \varphi_\mu^0(z) \to \varphi_\mu^1(z), \tag{9}$$

in such a way that the new ground subband wave function is pulled asymetrically towards the attractive donor layer. A lateral homogeneous perturbation, especially, causes no in-plane localization. Thus μ as well as $\vec{k}$ remain good quantum numbers.

In the final step we switch on the fluctuating part of the impurity potential:

$$H_{tot} = H_0 + eF_D z + V_{fl}(z,\vec{r}). \tag{10}$$

Since this perturbation couples the z and $\vec{r}$ coordinates, the Schrödinger equation is no longer separable. The translation symmetry parallel to the layers is destroyed and the plane-wave-type lateral wave functions are replaced by states with a complicated $\vec{r}$ dependence. However, if the typical width of the potential fluctuations $\triangle V_{fl}$ is not too large compared to the subband spacing of the undisturbed system, $\epsilon_{21}^0 = \epsilon_2^0 - \epsilon_1^0$, it can be expected that there remains some trace of the original subband structure in the perturbed electron gas. It is therefore reasonable to expand longitudinally in terms of the undisturbed quantum well eigenfunctions $\varphi_\mu^0(z)$:

$$\Psi_n(z,\vec{r}) = \sum_\mu \varphi_\mu^0(z)\,\phi_n^\mu(\vec{r}). \tag{11}$$

Thus, in the presence of disorder, due to the subband mixing, the electron states are in general a linear combination of various z-subband wave functions, each one attached to an individual 2D lateral function $\phi_n^\mu(\vec{r})$. The latter are determined by a set of coupled 2D Schrödinger equations:

$$\sum_\mu \left[\delta_{\nu\mu}\left(\frac{\mathbf{p}_r^2}{2m^\star}\right) + \langle \nu | V_{imp}(z,\vec{r}) | \mu \rangle \right] \phi_n^\mu(\vec{r}) = (E_n - \epsilon_\nu^0)\,\phi_n^\nu(\vec{r}), \tag{12}$$

where the effective 2D potentials are given as matrix elements of the 3D impurity potential with the undisturbed z-subband wave functions:

$$\langle \nu | V_{imp}(z,\vec{r}) | \mu \rangle = \int dz\, \varphi_\nu(z)\,\varphi_\mu(z)\,V_{imp}(z,\vec{r}). \tag{13}$$

B. Exact diagonalization

The coupled set of differential equations Eq. (12) has been transformed into a matrix equation by Fourier decomposition and then been diagonalized numerically. We thus expand the lateral functions further in terms of plane waves:

$$\phi_n^\mu(\vec{r}) = \sum_{\vec{k}} A_n^\mu(\vec{k})\, e^{i\vec{k}\vec{r}}. \tag{14}$$

Due to the periodic boundary conditions the wave vectors $\vec{k}$ are restricted to the discrete subset $\vec{k} = (k_x, k_y) = (2\pi/L) \times (u,v)$, with integers u and v. For the numerical implementation the basis had to be truncated, $u,v \in \{-k_{max}, \ldots, 0, \ldots, +k_{max}\}$, with $k_{max} = 12$ in most of the calculations below. The neglection of the high Fourier components is uncritical for not-too-thin spacer layers and for electron states with not-too-high kinetic energy. This is because the spacer layer exponentially suppresses the high Fourier components of the fluctuating impurity potential and because electronic wave functions with low kinetic energy can be accurately represented using only plane waves with small wave vectors. Also, here we have checked that a further increase of k_{max} yields no significant changes in the resulting eigenstates.

In k space the coupled Schrödinger equations (12) read

$$\sum_{\mu\vec{k}} \left[\delta_{\nu,\mu}\delta_{\vec{k}_2,\vec{k}}\left(\frac{\hbar^2 k^2}{2m^\star}\right) + \langle \vec{k}_2 \nu | V_{imp}(z,\vec{r}) | \vec{k}\mu \rangle \right] A_n^\mu(\vec{k}) = (E_n - \epsilon_\nu^0) A_n^\nu(\vec{k}_2), \tag{15}$$

with the potential matrix elements

$$\langle \vec{k}_2 \nu | V_{imp}(z,\vec{r}) | \vec{k}\mu \rangle = (1/L^2) \int d^2\vec{r}\, e^{-i(\vec{k}_2 - \vec{k})\vec{r}} \langle \nu | eF_D z + V_{fl}(z,\vec{r}) | \mu \rangle. \tag{16}$$

The latter can be calculated analytically, due to the simple trigonometric z wave functions, Eq. (7). For the homogeneous electric-field term one obtains

$$\langle \vec{k}_2 \nu | eFz | \vec{k}\mu \rangle = \delta_{\vec{k}_2,\vec{k}} \langle \nu | eFz | \mu \rangle = \delta_{\vec{k}_2,\vec{k}} \frac{eFa}{\pi^2}\left[\frac{(-1)^{\mu-\nu}-1}{(\mu-\nu)^2} - \frac{(-1)^{\mu+\nu}-1}{(\mu+\nu)^2} \right]. \tag{17}$$

For parity reasons, this part of the matrix element is nonzero only if $|\mu - \nu|$ is odd. The fluctuating part yields, using Eq. (4),

$$\langle \vec{k}_2 \nu | V_{fl}(z,\vec{r}) | \vec{k}\mu \rangle = \langle \nu | V_{fl}(z,\vec{q} = \vec{k}_2 - \vec{k}) | \mu \rangle = \langle \nu | V_0(z,\vec{q}) | \mu \rangle \cdot S(\vec{q}), \tag{18}$$

with the explicit single impurity term

$$\langle \nu | V_0(z,q) | \mu \rangle = \frac{2\pi K_0}{a} e^{-qd}\left[\frac{1-(-1)^{\nu+\mu}e^{-aq}}{q^2 + (\pi/a)^2(\nu+\mu)^2} - \frac{1-(-1)^{\nu-\mu}e^{-aq}}{q^2 + (\pi/a)^2(\nu-\mu)^2} \right]. \tag{19}$$

After diagonalizing the Hamiltonian matrix according to Eq. (15), the resulting coefficients $A_n^\mu(\vec{k})$ can be backtransformed to real-space wave functions $\Psi_n(z,\vec{r})$ with Eqs. (14) and (11), or can be used directly for calculating optical properties of the system.

In the dipole approximation, assuming the incident light polarized in the z direction, the intersubband absorption rate can be calculated using Fermi's golden rule:

$$\alpha(\hbar\omega)=\gamma_0\sum_{i,f}|\langle\Psi_f|p_z|\Psi_i\rangle|^2(f_i-f_f)\delta(E_f-E_i-\hbar\omega), \tag{20}$$

where f_i and f_f are the Fermi occupation probabilities of the initial and final state, at $T=0$ K determined by the Fermi level Φ_n:

$$f_n=\Theta(\Phi_n-E_n). \tag{21}$$

The constant prefactor γ_0 is state independent and has been set to 1. Note that, since the subband index and the wave vector are not good quantum numbers in the presence of disorder, the optical matrix elements can be nonzero for arbitrary pairs of states, in principle. The longitudinal electromagnetic field couples only to the z-dependent components of the wave function. Thus the optical transition amplitude can be written as

$$\langle\Psi_f|p_z|\Psi_i\rangle=\sum_{\nu,\mu}\langle\nu|p_z|\mu\rangle\langle\phi_f^\nu|\phi_i^\mu\rangle, \tag{22}$$

where the matrix elements between z subbands are explicitly given by

$$\langle\nu|p_z|\mu\rangle=-\frac{4i\hbar}{a}\cdot\frac{\mu\nu}{\nu^2-\mu^2}. \tag{23}$$

They are nonzero only between subbands of different parity. It is apparent from Eq. (22) that the transition amplitude depends on the spatial overlap $\langle\phi_f^\nu|\phi_i^\mu\rangle$ of the lateral wave functions. In the undisturbed system this overlap integral results in $\vec{k}$ conservation, since the lateral eigenfunctions are plane waves (vertical transitions in k space).

C. Local approximation

In addition to the above fully quantum-mechanical theory, we have studied a simple semiclassical model, which will be described in the following section. It is a straightforward application of the idea of calculating the absorption properties locally at each lateral position in the layer. Thus the 3D total potential experienced by the electrons, as defined in Eq. (1), is now interpreted as a 1D z profile, which depends on the in-plane position $\vec{r}_0$ only as a free *parameter*:

$$V_{loc}(z,[\vec{r}_0])=V_{tot}(z,\vec{r}_0). \tag{24}$$

For each $\vec{r}_0$ we solve the 1D Schrödinger equation *independently*,

$$[(p_z^2/2m^\star)+V_{loc}(z,[\vec{r}_0])]\varphi_\mu(z,[\vec{r}_0])=\epsilon_\mu[\vec{r}_0]\varphi_\mu(z,[\vec{r}_0]), \tag{25}$$

and calculate the local absorption coefficient for $\mu\rightarrow\nu$ transitions by

$$\begin{aligned}\alpha_{\mu\nu}(\hbar\omega,[\vec{r}_0])=&\gamma_1|\langle\varphi_\nu[\vec{r}_0]|p_z|\varphi_\mu[\vec{r}_0]\rangle|^2\\&\times(n_\nu^{(2)}[\vec{r}_0]-n_\mu^{(2)}[\vec{r}_0])\\&\times\delta(\epsilon_\nu[\vec{r}_0]-\epsilon_\mu[\vec{r}_0]-\hbar\omega).\end{aligned} \tag{26}$$

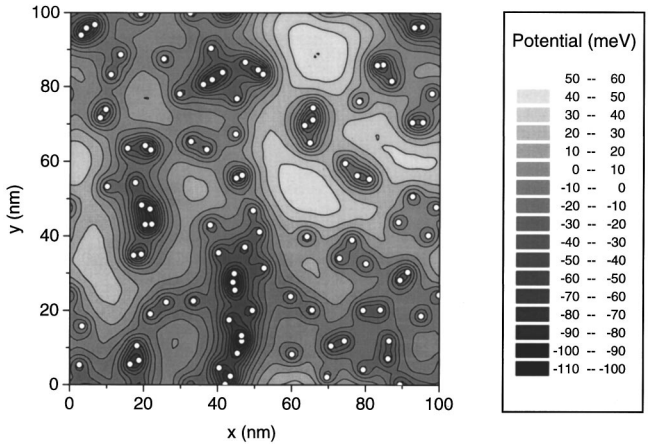

FIG. 2. Typical configuration of impurities (small circles) in the n layer and the resulting Coulomb potential at the left QW boundary ($z=0$). System parameters: $d=2$ nm, $N_D^{(2)}=10^{12}$ cm^{-2}.

Here $n_\mu^{(2)}[\vec{r}_0]$ is the 2D electron density of the μth subband at $\vec{r}_0$, which is at $T=0$ K given by

$$n_\mu^{(2)}[\vec{r}_0]=\frac{m^\star}{\pi\hbar^2}(\Phi_n-\epsilon_\mu[\vec{r}_0])\Theta(\Phi_n-\epsilon_\mu[\vec{r}_0]). \tag{27}$$

If we consider only $1\rightarrow2$ transitions, the local absorption is characterized by a single photon energy in this simple model,

$$\hbar\omega[\vec{r}_0]=\epsilon_2[\vec{r}_0]-\epsilon_1[\vec{r}_0], \tag{28}$$

and the inhomogeneous line broadening of the far-field spectrum is only due to the $\vec{r}_0$ dependence of the subband energy difference. It is obtained by averaging over the local spectra:

$$\alpha(\hbar\omega)=\gamma_2\int d^2\vec{r}_0\,\alpha_{12}(\hbar\omega,[\vec{r}_0]). \tag{29}$$

IV. RESULTS AND DISCUSSION

A. Potential fluctuations

To give an impression from the strong doping-induced potential fluctuations in systems with thin spacer layers, we have plotted a typical impurity distribution and the resulting lateral potential profile in Fig. 2. Throughout this paper, we assumed a doping density of $N_D^{(2)}=10^{12}$ cm^{-2} for the n layer. In the case of Fig. 2 the spacer layer thickness was $d=2$ nm. The contour lines of the potential correspond to the left quantum well boundary at $z=0$. Deep, narrow valleys are formed at donor clusters and relatively wide plateaus in regions of low impurity density. It should be mentioned that random potentials produced by charged centers are spatially correlated and obey a nontrivial probability distribution, in contrast to the typically used model potentials in more fundamental theoretical studies (e.g., δ correlated). We believe that the specific statistical properties of these profiles have a significant effect on the resulting electron states and should be accounted for, whenever comparison with experimental data is performed.

Ensemble-averaged probability distributions of the local potential in the $z=0$ plane are depicted in Fig. 3 for three

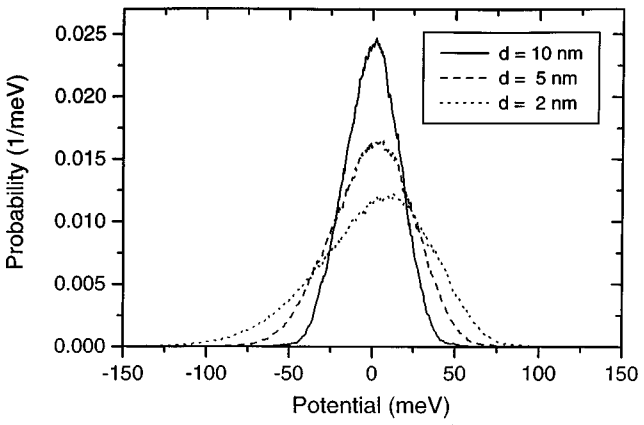

FIG. 3. Distribution function of the (unscreened) fluctuating potential in the $z=0$ plane for three different spacer layer thicknesses, averaged over 100 impurity configurations.

different widths of the spacer layer. It can be seen that the distribution function becomes Gaussian in the limit of large d. For thin spacer layers the distribution broadens and shows a strongly asymmetric shape with a long low-energy tail, a result of the deep potential minima mentioned above. Note that in the case of $d=2$ nm the full width at half-maximum (FWHM) is of the order of 100 meV.

B. Wave functions

Figure 4 gives two examples of wave functions calculated with the multisubband exact-diagonalization approach, for the case of the specific donor configuration of Fig. 2 and the standard system parameters $d=2$ nm and $a=10$ nm. We have used $k_{max}=12$ and four subbands in the calculation. The plotted point density is proportional to the lateral electron probability density, integrated over the z direction,

$$P_n(\vec{r})=\sum_{\mu} P_n^{\mu}(\vec{r})=\sum_{\mu} |\phi_n^{\mu}(\vec{r})|^2, \tag{30}$$

which has contributions from different subbands μ in general.

Part (a) depicts the ground state at an energy of $E_0=31.25$ meV, relative to the potential average at $z=0$. It is a nodeless wave function, localized at the global potential minimum of our simulation area. Its distribution in the z direction (not shown here) is asymmetric, with the maximum shifted from the QW center towards the attractive donor layer. The in-plane localization radius of excited wave functions generally grows with increasing energy, developing at the same time a complex structure of nodelines. See, e.g., Fig. 4(b), which shows the ninth excited state with energy $E_9=54.27$ meV.

C. Absorption line shape

On the basis of the exact disordered quantum states of a given impurity configuration, we computed the intersubband absorption spectrum according to Eq. (20). For determining the Fermi level Φ_n, an electron density of 2×10^{11} cm^{-2} has been assumed for all cases discussed below, corresponding to a filling factor $F=0.2$. The resulting absorption coefficient corresponds to a near-field spectrum of a small sample area with dimensions of 100 nm and therefore consists of a dense, but discrete distribution of δ peaks. To obtain a smooth far-field spectrum, we averaged over 30 different impurity configurations.

For our standard system parameters the resulting macroscopic absorption line is shown in Fig. 5, together with the semiclassical, local approximation. Note that the FWHM of the intersubband absorption peak is of order 1.5 meV, despite the potential fluctuations of about 100 meV. This remarkable difference will be discussed in detail below. The line shape is asymmetric with the longer tail at the high-energy side. It is found that these transitions are typically due to low-energy initial states, localized close to impurity clusters.

The overall agreement of the quantum-mechanical and semiclassical absorption spectra is surprising taking into account the crude approximation of the local model and its very low demands on computer resources. For the cases considered here, the peak position and asymmetry are reproduced nicely with the local approach, the FWHM is, however, slightly overestimated.

If the width of the QW is increased, keeping constant the spacer layer thickness, we observe a drastic broadening of the line and a larger discrepancy with the local model. See,

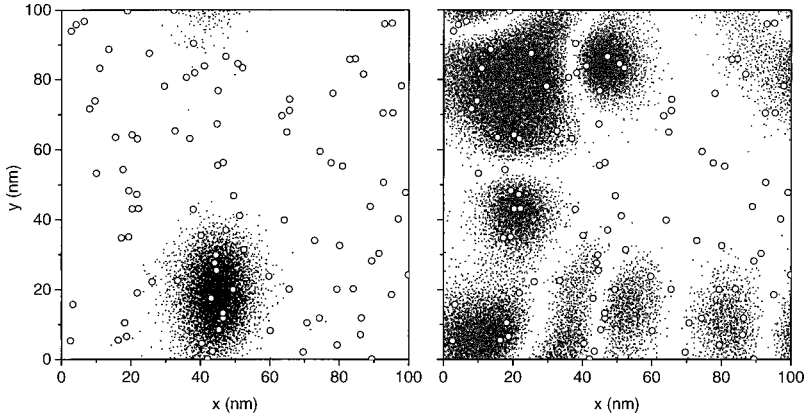

FIG. 4. Representative disordered electron states for the impurity configuration of Fig. 2. The point density is proportional to the in-plane probability density, averaged over the z direction. (a) Ground state with energy $E_0=31.25$ meV; (b) ninth excited state with energy $E_9=54.27$ meV.

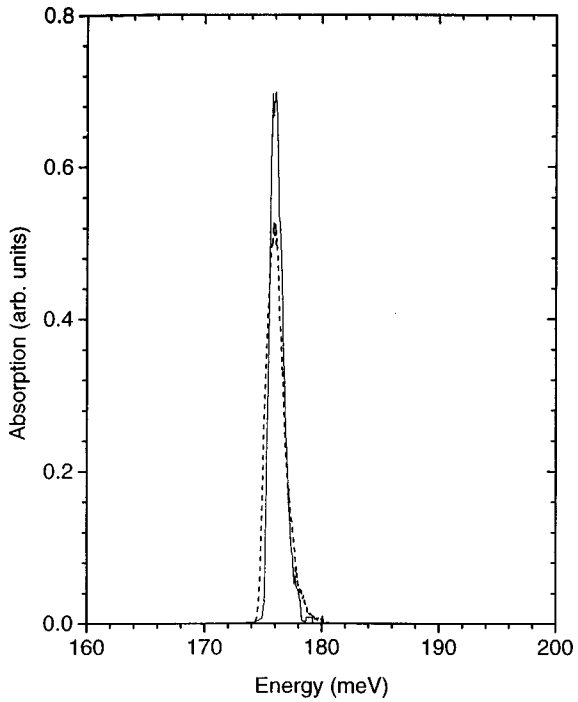

FIG. 5. Intersubband absorption spectrum for a system with $d=2$ nm, $a=10$ nm, and $F=0.2$. Solid line, exact diagonalization (FWHM$\approx$1.3 meV); Dotted line, local model (FWHM $\approx$1.7 meV).

e.g., Fig. 6, which corresponds to a 20-nm well, or the parameter dependence study in Fig. 7. On the other hand, the FWHM becomes as small as 0.07 meV in the case of $a=2$ nm.

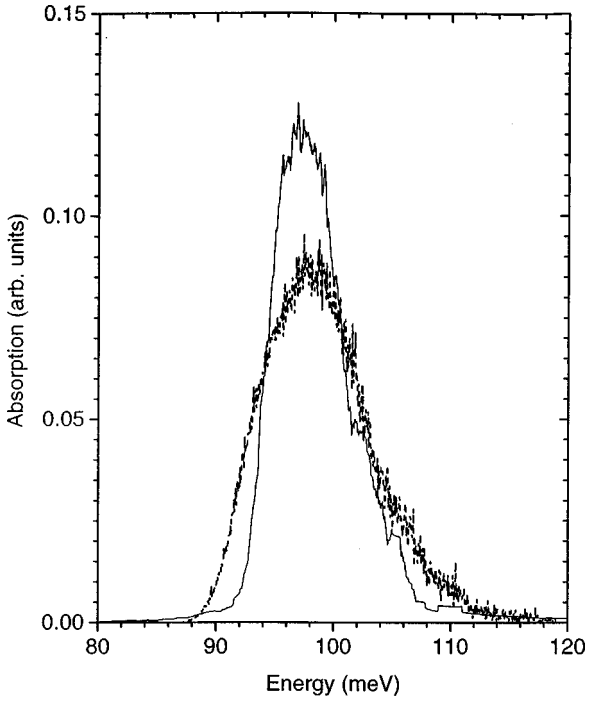

FIG. 6. Intersubband absorption spectrum for a system with $d=2$ nm, $a=20$ nm, and $F=0.2$. Solid line, exact diagonalization (FWHM$\approx$6.8 meV); dotted line, local model (FWHM $\approx$10.3 meV).

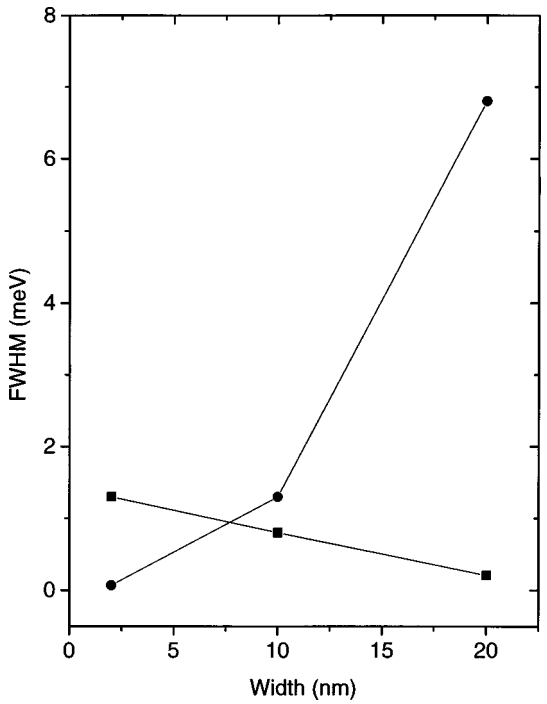

FIG. 7. Dependence of the FWHM of the absorption line on the quantum well width a and the spacer layer thickness d for a doping density of $N_D^{(2)}=10^{12}$ cm^{-2} and filling factor $F=0.2$. The lines are a guide for the eye. Circles, FWHM vs a for $d=2$ nm; squares, FWHM vs d for $a=10$ nm.

Figure 7 also contains the line width dependence on the spacer layer thickness for a QW with $d=10$ nm. The reduction of the disorder by removing the impurities is clearly visible, however the effect seems to be nonexponential. This is because the spatial separation only suppresses the short-wavelength components of the random potential. The remaining fluctuations with a correlation length of order $\lambda_{fl}=a$ are still capable of localizing electrons.

D. Semiclassical interpretation

The local model allows a very simple understanding of the main features of the intersubband absorption. In Fig. 8 we present the lateral distribution of the subband energy difference $\hbar\omega[\vec{r}_0]=\epsilon_1[\vec{r}_0]-\epsilon_0[\vec{r}_0]$ for a specific donor configuration (small circles) in the standard system. A clear correlation can be seen between the local impurity density and the absorption energy. Donor clusters cause a blue shift, producing the high energy wing in the spectrum, while the regions with low impurity density absorb at lower energy.

This can be semiquantitatively understood by considering only the constant and linear terms of the local z-potential profile in the QW region:

$$V_{loc}(z,[\vec{r}_0])\approx V_D[\vec{r}_0]+eF_D[\vec{r}_0]z. \tag{31}$$

The constant term has no net effect on the intersubband energy, since it shifts all subband edges by the same amount. The consequences of the linear longitudinal field term are well understood from the theory of the quantum confined Stark effect. With increasing F_D, the ground subband energy ϵ_1 is lowered (relative to the center of the QW bottom),

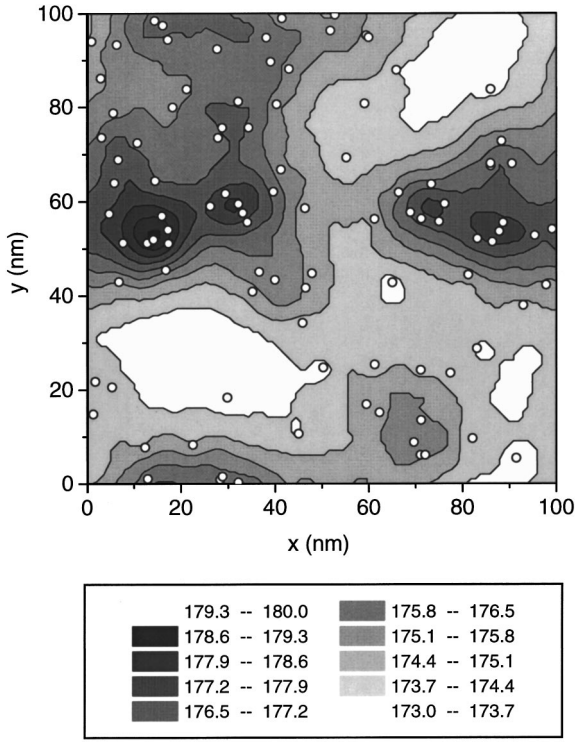

FIG. 8. In-plane distribution of the subband energy difference $\hbar\omega[\vec{r}_0]=\epsilon_2[\vec{r}_0]-\epsilon_1[\vec{r}_0]$ in the local model. Energies are given in units of meV. Impurities are represented by small circles. System parameters: $d=2$ nm, $a=10$ nm, $N_D^{(2)}=10^{12}$ cm^{-2}.

while the first excited subband ϵ_2 grows slightly in energy. This means that $\hbar\omega=\epsilon_1-\epsilon_0$ is a monotonously increasing function of F_D in the relevant field range.

We have plotted this dependence in Fig. 9 and marked the

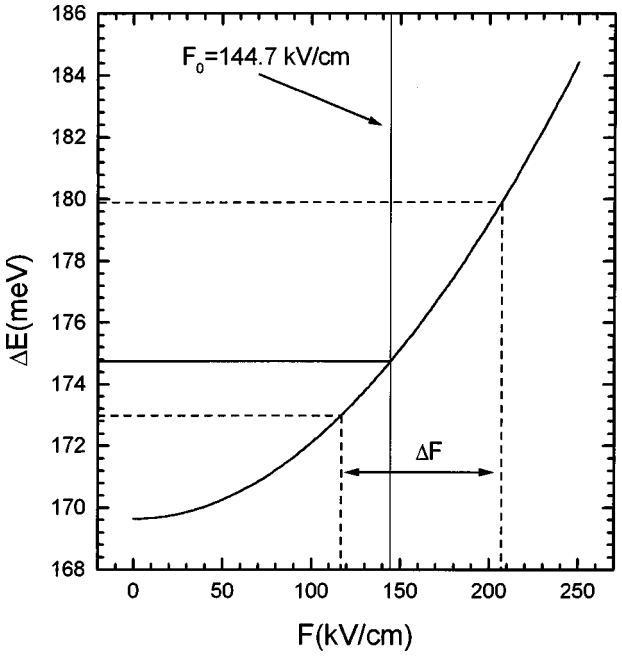

FIG. 9. Dependence of the subband energy difference $\epsilon_2-\epsilon_1$ on the electric field F_D. The solid vertical line corresponds to the average field, the dotted lines to its lateral fluctuation. System parameters: $d=2$ nm, $a=10$ nm, $N_D^{(2)}=10^{12}$ cm^{-2}.

average electric field with a solid vertical line. As a function of in-plane position $\vec{r}_0$, the local field is fluctuating around this value, roughly between the borders marked with broken lines. The *position-dependent Stark effect* causes a corresponding fluctuation of the intersubband energy, as shown in the figure. Note that the slope of the $\hbar\omega(F_D)$ dependence (the sensibility to field fluctuations) becomes steeper for wider QW's and zero in the extreme electric quantum limit $a\to 0$. This explains, semiclassically, the broadening of the spectra with increasing well width.

E. Correlation effect

We now analyze quantum mechanically the reason of the sharpness of the intersubband absorption spectra relative to the fluctuation width of the disorder potential. For this it is illuminating first to consider a thin quantum well with a thick spacer layer, $d>a$. In such a case the impurity potential at the QW has a correlation length of order d. Therefore, even if $V_{imp}(z,\vec{r})$ varies arbitrarily parallel to the layers and is strongly z dependent, we can assume *weak longitudinal fluctuations* and approximate Eq. (2) by

$$V_{imp}(z,\vec{r})=eF_Dz+V_{lat}(\vec{r}). \tag{32}$$

Obviously the total Hamiltonian can now be split into independent z- and $\vec{r}$-dependent parts,

$$\begin{aligned} H_{sep}&=H^z+H^{\vec{r}}\\ &=[(p_z^2/2m^\star)+V_{qw}(z)+eF_Dz]\\ &\quad+[(\mathbf{p}_r^2/2m^\star)+V_{lat}(\vec{r})] \end{aligned} \tag{33}$$

and its eigenstates are again separable,

$$\Psi_n(z,\vec{r})=\Psi_{\mu,m}(z,\vec{r})=\varphi_\mu^1(z)\,\phi_m(\vec{r}), \tag{34}$$

with well-defined z subbands, modified by the quantum confined Stark effect,

$$H^z\varphi_\mu^1(z)=\epsilon_\mu^1\varphi_\mu^1(z), \tag{35}$$

and disordered in-plane states,

$$H^{\vec{r}}\phi_m(\vec{r})=E_m\phi_m(\vec{r}). \tag{36}$$

For our hypothetical model case with purely lateral fluctuations we thus arrive at a density of states (DOS) in the conduction band,

$$D(E)=\sum_\mu D_{dis}(E-\epsilon_\mu^1), \tag{37}$$

which is a superposition of identical, disorder broadened subbands:

$$D_{dis}(E)=\Omega^{-1}\sum_m \delta(E-E_m). \tag{38}$$

The optical transition amplitude between two states [compare Eq. (22)] now reduces to

$$\langle\Psi_{\nu,n}|p_z|\Psi_{\mu,m}\rangle=\langle\nu|p_z|\mu\rangle\langle\phi_n|\phi_m\rangle=\langle\nu|p_z|\mu\rangle\delta_{m,n}. \tag{39}$$

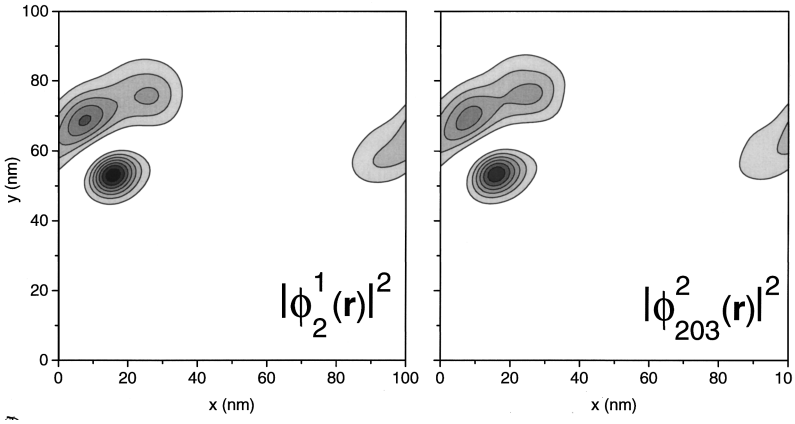

FIG. 10. Typical example of a pair of correlated in-plane wave functions. Shown is the z-averaged in-plane probability density of the functions ϕ^1_2 and ϕ^2_{203} with energies $E_2=21.48$ meV and $E_{203}=198.2$ meV, respectively. System parameters: $d=2$ nm, $a=10$ nm, $N_D^{(2)}=10^{12}$ cm^{-2}.

This means for the intersubband absorption with z-polarized light that for each given electron state $(1,m)$ in the ground subband there exists only one possible final state $(2,m=n)$ in the first excited subband. This single transition contains the whole oscillator strength and, independently from the initial state m, has a constant excitation energy $\hbar\omega=E_{2,m}-E_{1,m}=\epsilon_2-\epsilon_1$. Therefore, no matter how strong the lateral disorder is, the intersubband spectrum remains a δ peak. Note that the DOS and spectral properties of the system with purely lateral disorder are analogous to the QW without any disorder, where the subbands are step functions and the plane-wave-like lateral functions lead to the conservation of the k vector.

In reality the z dependence of the potential fluctuations cannot be completely neglected. However, for z-polarized light *the intersubband spectrum is sensitive only to the longitudinal potential fluctuations*, which are small for thin QW's. Then for each localized initial state Ψ_i (with dominating $\mu=1$ character) we expect that optical transitions can occur only into a small number of final states Ψ_f (of $\nu=2$ character) with energies $E_f\approx E_i+(\epsilon_2-\epsilon_1)$. One of them, $\Psi_{f(i)}$, will have a lateral overlap close to 1:

$$\langle\phi^2_{f(i)}|\phi^1_i\rangle\approx 1. \tag{40}$$

Since this specific transition $i\rightarrow f(i)$ gives the main contribution to the intersubband transition, we call Ψ_i and $\Psi_{f(i)}$ a *correlated pair of wave functions*.

We have found in our simulations that this strong lateral correlation of states, which are energetically separated by approximately the undisturbed subband distance, is a general feature of the quasi-2D electron gas under the influence of strong disorder. When intersubband mixing is weak, the electrons of the different subbands experience a very similar effective potential and thus develop similar in-plane wave functions. The resulting correlated pairs of states are localized at the same lateral positions and thus show almost the same energy shift from their corresponding undisturbed subband edges. In effect, the intersubband absorption is governed by vertical transitions in real space.

Typical examples of correlated pairs of wave functions are shown in Fig. 10 and Fig. 11. Note that the system parameters used for this calculation, $d=2$ nm and $a=10$ nm, are far from the ideal realization of purely lateral disorder. Nevertheless, the correlation of lateral wave functions is extremely well marked.

We can therefore trace back the sharpness of the intersubband absorption peak, relative to the huge random potential, to the insensitivity of the transition energies to lateral poten-

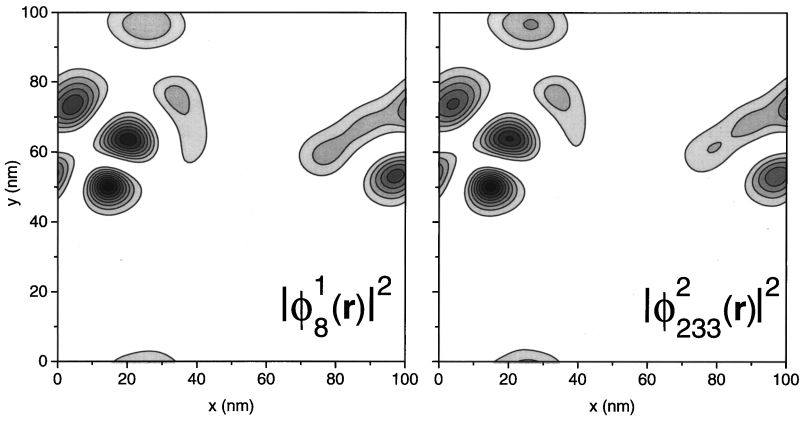

FIG. 11. z-averaged in-plane probability density of the functions ϕ^1_8 and ϕ^2_{233} with energies $E_8=38.22$ meV and $E_{203}=214.6$ meV, respectively. System parameters: $d=2$ nm, $a=10$ nm, $N_D^{(2)}=10^{12}$ cm^{-2}.

tial fluctuations. When the QW thickness a increases at constant d, longitudinal fluctuations become more pronounced and, consequently, a gradual broadening of the spectra is observed.

V. SUMMARY AND OUTLOOK

In summary we have performed a multisubband calculation of quasi-2D single-electron states under the presence of strong, doping-induced disorder. The one-particle intersubband excitation spectrum for constant filling factor as a function of QW width and spacer layer thickness has been computed on the basis of the numerically exact, disordered states and found to be extremely sharp in comparison to the lateral potential fluctuations. This result can be explained by the strong spatial correlations between states separated energetically by approximately the undisturbed subband distance. We have compared these results to a simple, semiclassical approximation and found a surprisingly good agreement despite the extreme simplifications made in the latter model.

We conclude that the correlations between quantum states are a general key feature of quasi-2D disordered multisubband systems and must be taken into consideration for a proper understanding of the intersubband absorption line shape. A similar effect may also be relevant for cyclotron resonance experiments in modulation-doped quantum wells, where the transitions are induced between localized states of different Landau levels.[10,11]

However, the results presented in this paper are not yet suitable for a direct comparison with experimental data. First of all, we used a simple model system with infinite barriers and neglected the interface roughness completely. In thin quantum wells, the width fluctuations may easily dominate the line broadening. While the presence of a positively charged impurity lowers the ground and first excited subband edges locally by a similar amount, an island of smaller well width increases the subband energy difference considerably in this region. For example in Ref. 3, an increase of the linewidth from 2.6 meV to 4.4 meV was reported for a series of modulation-doped ($d=20$ nm) quantum wells of widths ranging between 11 nm and 7.5 nm, respectively. It would be straightforward to include interface roughness into our model, as has already been realized in a recent study on exciton localization.[12]

Second, it is well known that electron-electron interactions play a crucial role for the intersubband absorption process, becoming of course more pronounced with increasing carrier density. The static screening reduces the effective potential fluctuations and thus leads to a narrowing of the absorption line in the single-particle picture. The dynamic interaction of the electrons, which form a system of coupled oscillators, enables a collective response to the perturbing light field. This leads at low excitation power to a blueshift of the peak (depolarization shift).[1] For an excitation power comparable to the saturation intensity, however, the second subband becomes populated, the depolarization shift is reduced again and a more complicated line distortion is observed experimentally.[2]

The inclusion of these many particle effects into the theoretical model represents the next step towards a realistic simulation of the intersubband absorption process in disordered systems. The authors have already extended the model to the case of doping superlattices with electrically tunable carrier density. These systems are free of interfaces and form an extreme case of well-controlled disorder, since the electrons are directly exposed to the charged donors. Static screening has been accounted for by a self-consistent Hartree calculation of the single-particle quantum states. The dynamic screening effects can be included by a natural extension of Ando's linear response theory[1] to the case of localized oscillators. These results will be published elsewhere.

ACKNOWLEDGMENTS

One of the authors (C.M.) would like to thank the Deutsche Forschungsgemeinschaft DFG for financial support and S. Tsujino and M. Beck for stimulating discussions.

[1] T. Ando, A. B. Fowler, and F. Stern, Rev. Mod. Phys. **54**, 437 (1982).
[2] K. Craig, B. Galdrikian, J. Heyman, A. Markelz, J. Williams, M. Sherwin, K. Campman, P. Hopkins, and A. Gossard, Phys. Rev. Lett. **76**, 2382 (1996).
[3] K. Campman, H. Schmidt, A. Imamoglu, and A. Gossard, Appl. Phys. Lett. **69**, 2554 (1996).
[4] E. Dupont, D. Delacourt, D. Papillon, J. Schnell, and M. Papuchon, Appl. Phys. Lett. **60**, 2121 (1992).
[5] M. Zaluzny, Phys. Rev. B **43**, 4511 (1991).
[6] T. Ando, Z. Phys. B **26**, 263 (1977).
[7] R. J. Warburton, C. Gauer, A. Wixforth, J. P. Kotthaus, B. Brar, and H. Kroemer, Superlattices Microstruct. **19**, 366 (1996).
[8] T. Ando, J. Phys. Soc. Jpn. **54**, 2671 (1985).
[9] K. Schrüfer, C. Metzner, M. Hofmann, and G. H. Döhler, Superlattices Microstruct. **21**, 2 (1997).
[10] U. Merkt, Phys. Rev. Lett. **76**, 1134 (1996).
[11] E. Batke, G. Weimann, and W. Schlapp, Phys. Rev. B **43**, 6812 (1991).
[12] C. Metzner, G. Döhler, and H. Sakaki, Phys. Status Solidi A **164**, 471 (1997).